E|DPC-2016

Electric Drives Production Conference 2016

6th International Conference

Electric Drives Production

November 30th – December 1st, 2016
Nuremberg, Germany

Proceedings

MARSILLI

Bühler Motor

ZIEHL-ABEGG

TEMPEL

AMA Verband für Sensorik + Messtechnik

ECPE

EMCW

UK Magnetic Society

BEM eMobilität

antriebstechnik

Automation Valley Nord-Bayern

Bayern Innovativ

MHI Wissenschaftliche Gesellschaft Montage Handhabung Industrierobotik

BÜHLER MOTOR MECHATRONIC AWARD 2016

cluster mechatronik & automation

ETG Power Engineering Society within VDE

VDE

FAPS

FVA Forschungsvereinigung Antriebstechnik e.V.

metropolregion nürnberg SEE IT. FEEL IT. STAY.

pels IEEE Power Electronics Society Powering a Sustainable Future

IHK Industrie- und Handelskammer Nürnberg für Mittelfranken

conf Make your conference easy

IEEE

VDMA Antriebstechnik

Green Factory BAVARIA

E|Home-Center Bavarian Technology Center for Domestic Living

E|Drive-Center Bayerisches Technologiezentrum für elektrische Antriebstechnik

Influence of Axial Mechanical Stress on the Magnetic Properties of Non-Oriented Electrical Steel

G. von Pfingsten and K. Hameyer, *Sen. Member IEEE*
Institute of Electrical Machines (IEM)
RWTH Aachen University
Schinkelstr. 4, 52062 Aachen, Germany
georg.vonpfingsten@iem.rwth-aachen.de

D. Paul
ThyssenKrupp Presta Camshafts
Heinrich-Lorenz-Str. 57, 09120 Chemnitz, Germany
daniel.paul@thyssenkrupp.com

***Abstract*—Axial mechanical stress on electrical steel significantly affects the magnetic properties of electric steel. The magnetizability is reduced and the losses are increased. In electrical machines, axial mechanical stress is induced in different processes of production. The lamination stacks are often compressed by means of axial pressure to create a compact and robust magnetic core. This work focuses on the influence of axial pressure on the rotor lamination stack from a new low cost rotor assembly. A setup is constructed to measure the influence of axial mechanical pressure on the magnetic properties of ring core samples made of electric steel. Extensive measurements at different values of axial mechanical pressure are conducted. From the measured data, an iron loss model is parametrized. The influence of axial mechanical pressure on the hysteresis losses and the eddy current losses is discussed. The identified loss model parameters are applied to the solution of a 2D FEM simulation of the permanent magnet synchronous machine. The influence on the loss characteristics of the machine is studied.**

Keywords— Electrical Machines, Electrical Steel, Mechanical Stress, Mechanical Pressure, Magnetic Properies, Ring Core Measurements

I. Introduction

Axial mechanical pressure on electrical steel can negatively affect the magnetization and loss behavior. Due to the production process, axial stress occurs in induction machines with die casted rotor cage, which inherently bears axial load on the rotor laminations. In the production process of electrical machines, the stack of electrical steel sheets is often compressed by means of axial pressure in order to create a compact and mechanically robust magnetic core. Many papers study the influence of mechanical stress in laminar direction of electrical steel [1 - 7]. [1] studies the excess eddy current losses from mechanical pressure in laminar direction. In [2 - 4], measurements of the flux density in the two laminar dimensions are conducted. In [5, 6], the influence of mechanical stress in laminar direction from shrink fitting on the characteristics of a permanent magnet synchronous machine (PMSM) is simulated. In [6], a setup to measure the influence of stress in laminar direction from shrink fitting is presented. Measurements of the influence of shrink fitting on the magnetization curve are conducted.

A few papers deal with the influence of stress normal to the lamination direction on the magnetic properties of electric steel. In [8], one lamination ring of electric steel is measured under axial pressure. Hence, no effects that occur from putting multiple steel rings under pressure is addressed. In [9], ring cores of electric steel are measured under pressure in axial directions. Depending on the value of magnetic flux density, the eddy current losses are either increased or decreased from axial stress [9]. In [7], the influence of axial stress on the stator of a 30 kW PMSM is studied. The soft magnetic measurement results from [7] indicate a slight increase of the iron losses at 50 Hz and 1.5 T when applying axial pressure. With the application of 4 MPa of axial pressure on the stator stack, an increase of 3.6 % of the iron losses is modeled in [7].

In this paper, we study the effect of axial pressure on electrical steel laminations by means of ring core measurements. A test setup is constructed for this purpose. Soft magnetic measurements at different values of applied axial pressure σ and different frequencies f are conducted.

It will be shown, that the influence of axial pressure on the core losses is highly dependent on the inter-laminar short circuit paths due to burrs from cutting. The literature on measurement of the influence of cutting burrs treats cutting burrs by adding artificial short-circuit paths on the edges of the laminations [10, 11]. In contrast to this, we will study the influence of inter-laminar short circuit by burrs created by axial pressure on the lamination stack.

II. Axially Clamped Rotor Assembly

Intention of a research project which is studied by ThyssenKrupp Presta Camshafts is to use electrical steel sheets mechanically for an innovative rotor architecture. Though it has to be taken into account not to compromise the electromagnetic behavior. In the first place, motivation of applying axial load onto rotor laminations will be analyzed in order to derive pressure data for further investigation. Though state of the art rotor layouts often show pressure discs on either side, the axial press force is uncertain and differs largely. In addition to using side plates for balancing, there are two reasons for such rotor design with axial press force. First is to prevent lamination sheets from fanning out while operation. Most common method for rotor laminations is interlocking. Such stack built incorporates air gaps between single sheets and therefore some amount of spring back which causes a loss of density in active material. Thus, the second purpose of axial clamping is to increase the packing density.

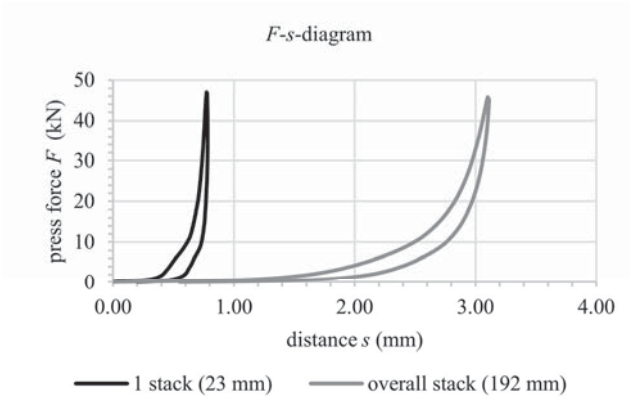

Fig. 1: Compression of lamination stacks produced by interlocking.

The compression behavior is studied on an example with single stack 23 mm and overall rotor stack length of 192 mm (Fig. 1). The investigation not only results in evaluating required press forces but also leads to a certain elastic spring characteristic with a given spring ratio. This property can be well used mechanically for an alternative rotor design with air gap between shaft and lamination stack. Alike arrangement is applied for patent DE102014106614 (Fig. 2).

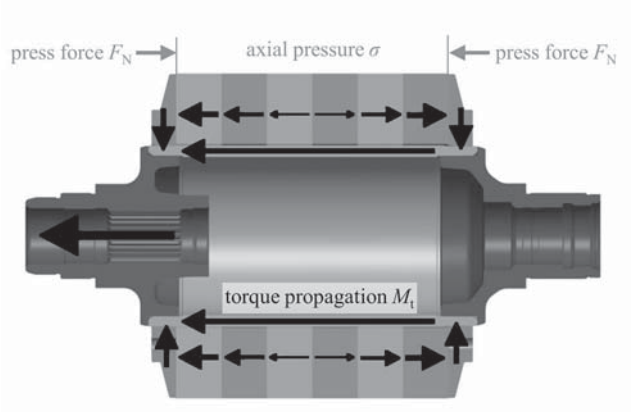

Fig. 2: Axially clamped rotor assembly according to DE102014106614.

The design features torque transmission via axial compression discs by means of frictional locking instead of the industry standard shrink-fitting of rotor laminations and shaft. Thus, the compression discs bear axial pressure on the electric steel stack. Given a known adhesion friction coefficient, the required press force can be calculated. Due to geometrical and mechanical constraints there is no even distribution of that force on the laminations. FEM modelled geometry can be used to determine areas of different axial pressure. Structural analysis shows a general decrease of load from inner to outer diameter (Fig. 3). As pressure discs are only fixed on the inner diameter, their stiffness leads to the effect detected. In addition any geometrical cutout such as, magnet pockets, interlockings or air cooling channels contribute to amplify axial loads on remaining areas.

The machine studied with 200 Nm torque and a friction coefficient of $\mu > 0.27$ required about 45 kN axial press load:

$$F_R = F \times \mu = 45{,}000\ \text{N} \times 0.27 = 12{,}150\ \text{N}$$
$$\Rightarrow M_t = F_R \times r_R = 12{,}150\ \text{N} \times 0.053\ \text{m} = 644\ \text{Nm}. \quad (1)$$

Applying this load onto an axial surface area of the lamination leads to an average pressure of:

$$\sigma = \frac{F}{A} = \frac{45{,}000\ \text{N}}{8{,}300\ \text{mm}^2} = 5.42\ \text{MPa}. \quad (2)$$

With consideration of uneven distribution and pressure mapping by structural analysis, a range of 2 - 10 MPa is defined for measuring magnetic properties.

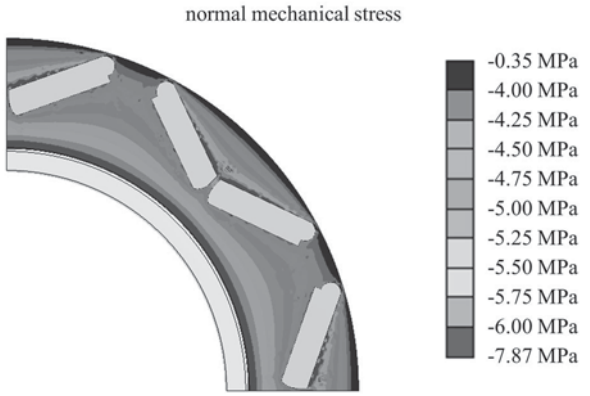

Fig. 3: Static mechanical FEM simulation of axial pressure on lamination.

III. Soft Magnetic Measurement Setup

Standardized measuring configurations are not suitable to measure magnetic properties of electric steel under axial pressure. Single-Sheet and Epstein configurations do not allow the application of force to the specimen. The application of axial force on standard ring-core specimens would lead to high forces on the primary and secondary winding. The forces may damage the windings. When applying force on the windings, the force distribution in the electric steel is dependent on the exact wire positions and wire dimensions. An even local distribution of force in the electric steel cannot be guaranteed. Hence, a special measurement setup is used (Fig. 4). The measured specimen is a ring core which is inserted in a winding body. Primary and secondary winding are inserted into slots of the winding body. In this way, axial force can be applied to the winding body without applying force to the windings. The structure of the winding body is sketched in Fig. 5. The winding body with inserted electric steel rings and windings is put into a hydraulic press allowing to apply axial force. The force is measured using a force transducer. The hydraulic press is adjusted manually to create the desired force F. A force value of $F = 34.6$ kN equals an applied axial compressive pressure in the electric steel rings of $\sigma = 10$ MPa.

IV. Measurement Results

Soft magnetic measurements are conducted under sinusoidal flux density waveform for different magnetizing frequencies f, flux density magnitude B and values of axial compressive pressure σ. The maximum value of the applied axial pressure is $\sigma = 10$ MPa. A *Brockhaus MPG 200* system is used for the soft magnetic measurements.

A. Permanent influence of applied axial pressure

The measurement procedure starts with the lowest value of $\sigma = 0$ MPa and ends with the highest axial pressure of

$\sigma = 10$ MPa. After the application of $\sigma = 10$ MPa, the hydraulic press is released, i.e. no pressure is applied ($\sigma = 0$ MPa). The soft magnetic measurements are repeated at $\sigma = 0$ MPa. The measurements at $\sigma = 0$ MPa before and after applying the maximum axial pressure of $\sigma = 10$ MPa revealed no significant difference in magnetizability or iron losses. Hence, the influence axial mechanical pressure of $\sigma \leq 10$ MPa for short time periods does not permanently degrade the magnetic properties of electric steel.

B. *Magnetizability*

The magnetizability $B_{max}(H_{max})$ for 50 Hz is shown in Fig. 6. The measurement data shows an increase of the magnetic field strength H_{max} which is necessary for a given maximum flux density B_{max}. Fig. 7 shows the maximum increase $\Delta H_{max}(\sigma)$ of the necessary value of H_{max}:

$$\Delta H_{max}(\sigma) = \max_{B_{max}} H_{max}(\sigma, B_{max}) - H_{max}(\sigma = 0 \text{ MPa}, B_{max}). \quad (3)$$

The maximum value for ΔH_{max} of 371 A/m is measured at $B_{max} = 1.3 \ldots 1.4$ T. The increase of the maximum necessary field strength $\Delta H_{max}(\sigma)$ is almost linear with the axial mechanical pressure σ up to the maximum measured value of $\sigma = 10$ MPa. The maximum relative increase of the necessary magnetic field strength $\Delta H_{max,rel}$ is shown in Fig. 7:

$$\Delta H_{max,rel}(\sigma) = \max_{B_{max}} \frac{H_{max}(\sigma, B_{max}) - H_{max}(\sigma = 0 \text{ MPa}, B_{max})}{H_{max}(\sigma = 0 \text{ MPa}, B_{max})}. \quad (4)$$

The maximum values of $\Delta H_{max,rel}$ are all found at $B_{max} = 1.1$ T. The maximum relative increase $\Delta H_{max,rel}$ of 68.8 % is found at the maximum value of σ. The increase ΔH_{max} and relative increase $\Delta H_{max,rel}$ of the magnetic field strength are almost linear with the axial mechanical pressure σ up to the maximum measured value of $\sigma = 10$ MPa. The magnetization behavior of the electric steel is reduced under the application of axial mechanical pressure. The magnetization reduction is most significant at medium values of magnetic flux density (Fig. 6). At high values of magnetic field strength, i.e. saturation, the influence of pressure on the magnetization characteristics is small.

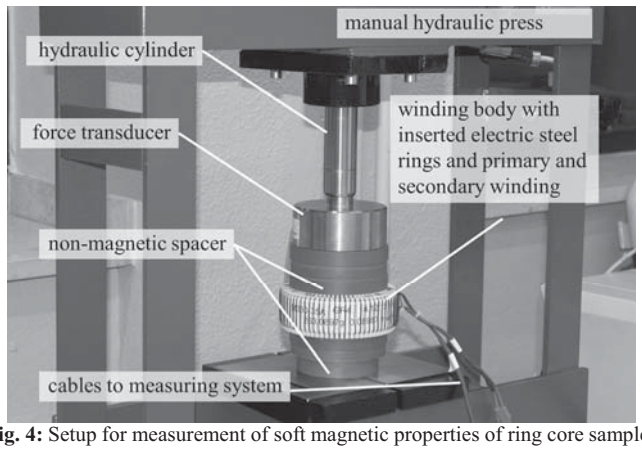

Fig. 4: Setup for measurement of soft magnetic properties of ring core samples while applying a force normal to the laminar direction.

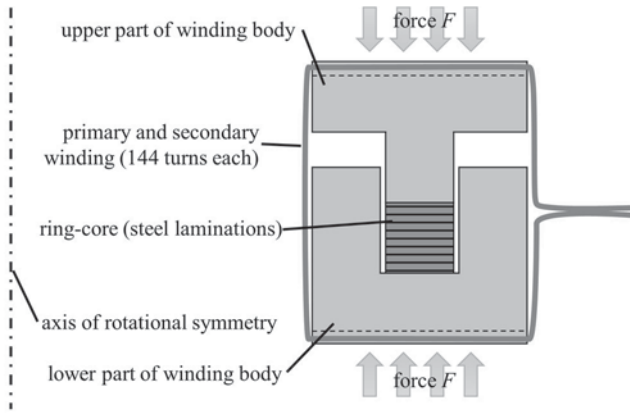

Fig. 5: Cross section of measurement setup consisting of the winding bodies, primary and secondary winding and the ring-core sample of steel laminations.

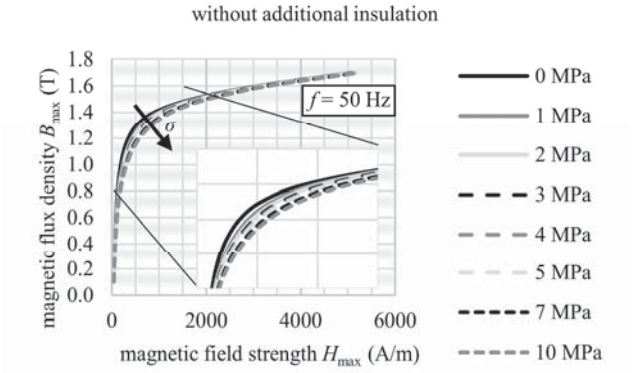

Fig. 6: Measured magnetizability of *M330-35A* for different values of axial pressure normal to laminar direction.

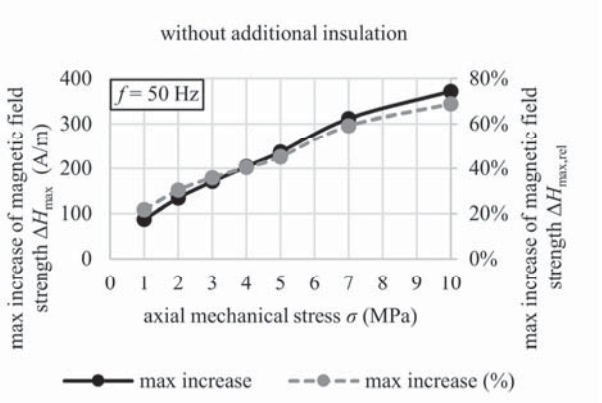

Fig. 7: Maximum measured increase of magnetic field strength (ΔH_{max} at $B_{max} = 1.3 \ldots 1.4$ T, $\Delta H_{max,rel}$ at $B_{max} = 1.1$ T).

C. *Hysteresis Losses*

The influence of mechanical pressure on the hysteresis is studied. Fig. 8 shows hysteresis curves at different values of mechanical pressure. From Fig. 8 it is observed, that the increase of the area of the magnetization curve is small. Mainly the magnetization curve is sheared to higher magnetic field strength values H_{max}. Fig. 9 shows the DC energy E_{hy} of the hysteresis loops in dependency of the axial mechanical pressure σ.

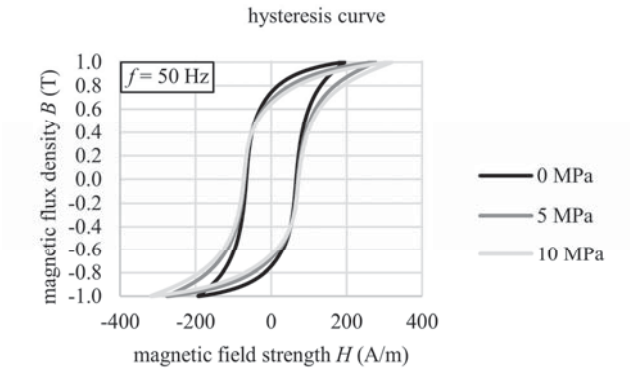

Fig. 8: Measured hysteresis curve at three different values of axial pressure σ.

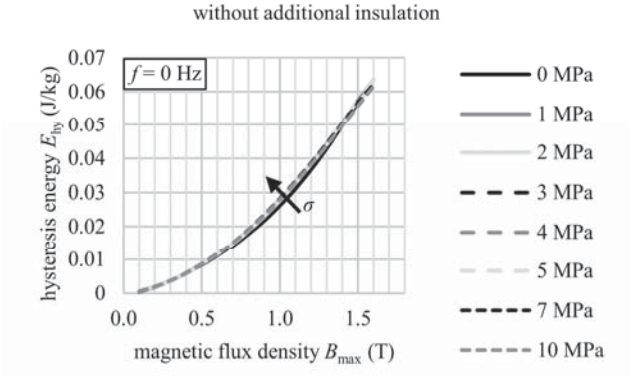

Fig. 9: Measured DC energy of *M330-35A* for different values of mechanical pressure normal to laminar direction.

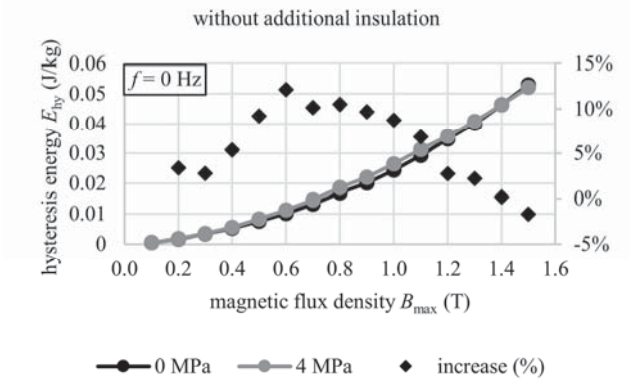

Fig. 10: Measured DC energy of *M330-35A* for σ = 0 MPa and σ = 4 MPa.

Fig. 10 shows the measured DC energy E_{hy} in dependency of the magnetic flux density B_{max} for the two values of axial pressure $\sigma = 0$ MPa and $\sigma = 4$ MPa. At medium values of $B_{max} = 0.5$ T … 1.0 T, E_{hy} increases approx. 10 %. The maximum increase ΔE_{hy} from $\sigma = 0$ MPa to $\sigma = 4$ MPa of 2.13 mJ/kg is measured at $B_{max} = 1.0$ T. The maximum relative increase of 12.1 % is measured at $B_{max} = 0.6$ T. At high values of magnetic flux density $B_{max} > 1.2$ T, the measured hysteresis losses are almost independent of the axial pressure σ.

The maximum increase of the measured DC hysteresis energy $\Delta E_{hy,max}$ is evaluated as:

$$\Delta E_{hy,\,max} = \max_{B_{max}} E_{hy}(\sigma, B_{max}) - E_{hy}(\sigma = 0\ \text{MPa}, B_{max}). \quad (5)$$

The value of B_{max}, at which $\Delta E_{hy,max}$ is found, is 1.0 T for all measured values of σ. The maximum DC energy increase is between $\Delta E_{hy,max} = 1.63$ mJ/kg and 2.13 mJ/kg and shows no distinct behavior with axial pressure σ. The value of the hysteresis energy E_{hy} without axial pressure ($\sigma = 0$ MPa) is $E_{hy}(0\ \text{MPa}, 1.0\ \text{T}) = 24.32$ mJ/kg. From E_{hy}, the specific hysteresis losses p_{hy} at sinusoidal magnetic flux density waveform with the frequency f can be calculated as:

$$p_{hy} = E_{hy} \cdot f. \quad (6)$$

Hence, at $f = 50$ Hz the maximum specific hysteresis loss increase from axial pressure is 0.11 W/kg. At $f = 2$ kHz, the maximum loss increase due to increased hysteresis losses would be 4.26 W/kg. Hence, the iron losses are only slightly influenced by the DC hysteresis loss component increase due to mechanical pressure in axial direction. Since most of the iron losses in the rotor of IM and PMSM are created by harmonics and therefore at higher frequencies, the hysteresis losses will have no strong impact on the machine losses. However, for an appropriate parameter identification of the eddy current losses, a precise description of the DC hysteresis losses is necessary. In the following, the losses at high frequency are analyzed.

D. Eddy Current Losses

To determine the influence of frequency f and axial pressure σ, the losses are measured at $f = 50$ Hz, 100 Hz, 200 Hz, 400 Hz, 1 kHz and 2 kHz. From the measurement data, the parameters of a loss model are determined. From the loss model parameters, the influence of axial pressure on eddy current losses is derived. To find the influence of inter-laminar short-circuit current paths (Fig. 11) from cutting burrs on the losses, the following measurements are conducted:

(a) without additional insulation layer (six weeks after cutting the electric steel by water-jet),

(b) without additional insulation layer (six months after cutting the electric steel by water-jet),

(c) after applying a 60 µm additional insulation layer,

(d) after removal of the cutting burrs.

The measured losses (a) at high frequency show a significant increase due to axial pressure. At 1 kHz (Fig. 12), an increase from 49.4 W/kg to 71.2 W/kg (+44 %) due to axial pressure of $\sigma = 5$ MPa is measured. At 2 kHz an increase of 75.5 W/kg to 116.0 W/kg (+53.6 %) is measured. This increase cannot be caused by influence of hysteresis losses, since the increase of the hysteresis losses at $f = 2$ kHz would be less than 4.26 W/kg (Sec. C). Table I gives the measured loss data at high frequency. Fig. 12 - 15 show the measured losses at $f = 1$ kHz for the cases (a), (b), (c) and (d) in dependency of σ and B_{max}.

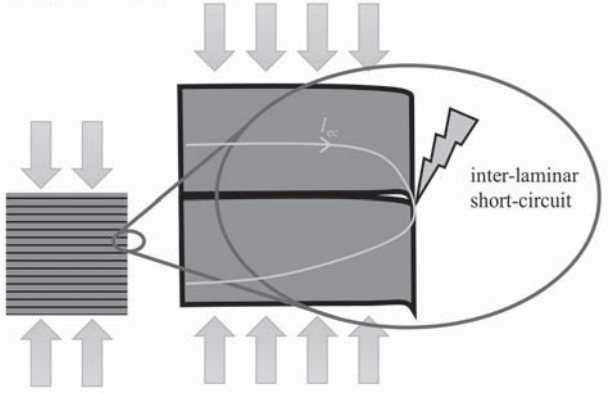

Fig. 11: Inter-laminar short-circuit from axial pressure and cutting burr.

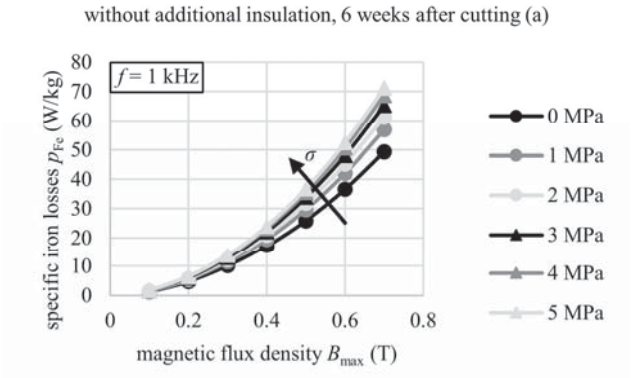

Fig. 12: Measured specific iron losses at $f = 1$ kHz with influence of additional eddy current due to cutting burrs (6 weeks after cutting).

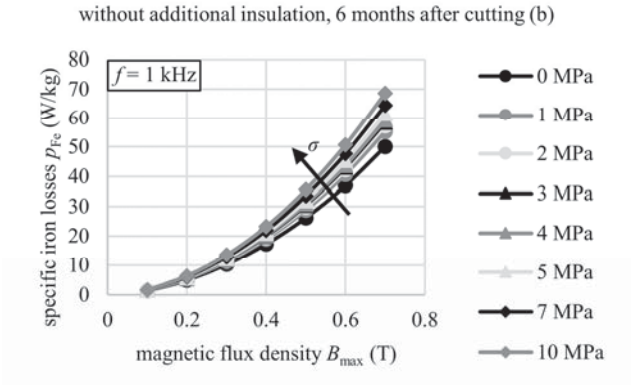

Fig. 13: Measured specific iron losses at $f = 1$ kHz with influence of additional eddy current due to cutting burrs (6 months after cutting).

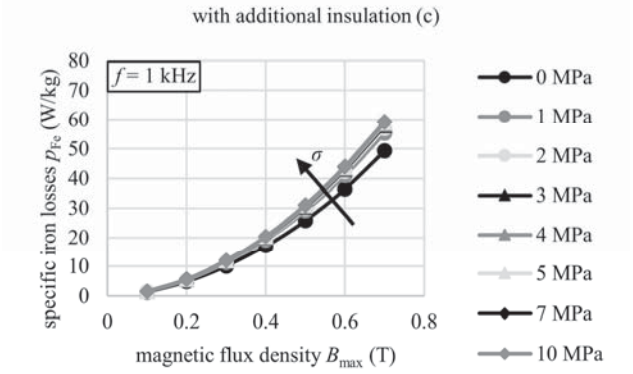

Fig. 14: Measured specific iron losses at $f = 1$ kHz after applying the 60 µm additional insulation layers.

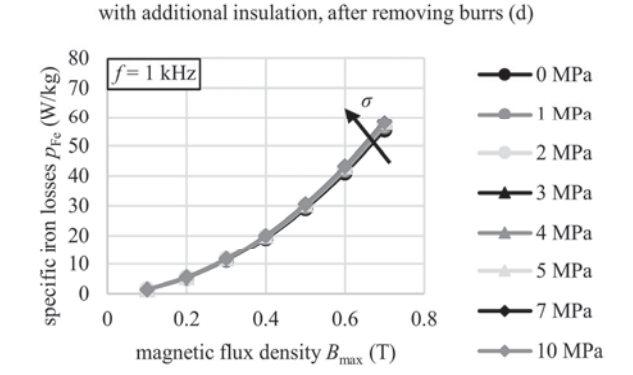

Fig. 15: Measured specific iron losses at $f = 1$ kHz after removing the cutting burrs and adding the second insulation layer.

TABLE I. INFLUENCE OF AXIAL PRESSURE ON MEASURED SPECIFIC IRON LOSSES AT HIGH FREQUENCY

axial pressure σ:		**0 MPa**	**5 MPa**	**10 MPa**
measurement		measured losses in W/kg		
a)	$f = 1$ kHz, $B_{max} = 0.7$ T	49.42	71.17	-
a)	$f = 2$ kHz, $B_{max} = 0.5$ T	75.45	116.02	-
b)	$f = 1$ kHz, $B_{max} = 0.7$ T	48.48	61.31	68.64 (+41.6 %)
b)	$f = 2$ kHz, $B_{max} = 0.5$ T	73.81	97.27	111.84 (+51.5 %)
c)	$f = 1$ kHz, $B_{max} = 0.7$ T	49.36	58.93	59.38 (+20.3 %)
c)	$f = 2$ kHz, $B_{max} = 0.5$ T	75.51	93.12	94.42 (+25.0 %)
d)	$f = 1$ kHz, $B_{max} = 0.7$ T	55.32	57.98	58.00 (+4.8 %)
d)	$f = 2$ kHz, $B_{max} = 0.5$ T	85.58	91.20	91.92 (+7.4 %)

Commonly, the iron losses are differentiated into the hysteresis loss component and eddy current losses. Since the loss increase at high frequency due to axial pressure cannot be explained by increased hysteresis component, eddy currents (microscopic and macroscopic) are studied as a possible cause.

Excess eddy current losses

To study the influence on microscopic (excess) and macroscopic (Foucault) eddy currents, the following iron loss model is fitted to the material measurements:

$$E_{\text{model}}(\sigma, B_{\max}, f) = E_{\text{hy}}(\sigma, B_{\max}) + k_{\text{ex}}(\sigma) B_{\max}^{1.5} f^{0.5} + k_{\text{cl}}(\sigma) B_{\max}^{2} f. \quad (7)$$

The loss model parameters k_{ex} and k_{cl} are found by solving the minimization problem:

$$\min_{k_{\text{ex}}(\sigma), k_{\text{ec}}(\sigma)} \left(\sum \left(E_{\text{model}}(k_{\text{ex}}(\sigma), k_{\text{cl}}(\sigma)) - E_{\text{meas}} \right)^2 \right). \quad (8)$$

The identified value of the excess loss parameter k_{ex} is shown in Fig. 16. $k_{\text{ex}}(\sigma)$ varies between 0.6 mW·kg^{-1}·T$^{-1.5}$·s$^{-1.5}$ and 0.78 mW·kg^{-1}·T$^{-1.5}$·s$^{-1.5}$. As shown in Fig. 10, the identified value of the excess loss parameter k_{ex} does not show a distinct dependency of the value of axial pressure σ.

A fixed value of $k_{\text{ex}} = 0.7$ mW·kg^{-1}·T$^{-1.5}$·s$^{-1.5}$ increases the square fitting error from (6) less than 1.8 % for all measured data sets. Hence, $k_{\text{ex}} = 0.7$ mW·kg^{-1}·T$^{-1.5}$·s$^{-1.5}$ is set for all values of σ for all sample sets (a,b,c,d). The excess eddy current losses are identified as independent of the axial pressure σ.

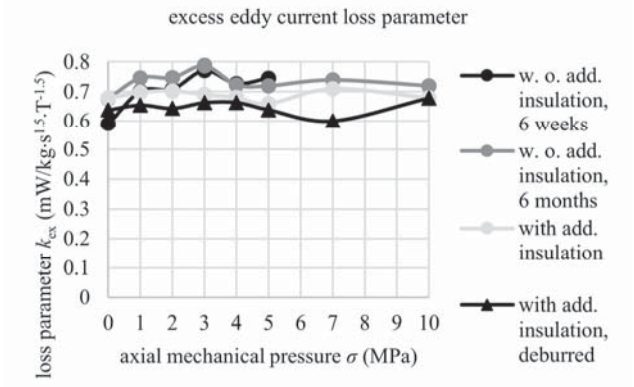

Fig. 16: Excess loss parameter determined according to (6).

Foucault eddy current losses

Since no significant relationship between the excess losses and axial pressure was found, the fitting from (8) is repeated using a constant value of $k_{ex} = 0.7\ \mathrm{mW \cdot kg^{-1} \cdot T^{-1.5} \cdot s^{-1.5}}$ leading to the following formulation:

$$\min_{k_{ec}(\sigma)} \left(\sum \left(E_{model}(k_{ex}, k_{cl}(\sigma)) - E_{meas} \right)^2 \right). \quad (9)$$

The area around the cutting edge is deformed from cutting (burr). The sample rings were prepared by waterjet cutting. The cutting burr was measured on all rings by an outside micrometer. A maximum height of the burr of 60 µm was measured. When pressurizing two or more electrical steel sheets, these cutting burrs lead to short circuit paths between the laminations (Fig. 11). Thus higher macroscopic eddy currents occur.

As the additional eddy current I_{ec} is conducted by the contact of the cutting burrs, I_{ec} and the additional losses resulting from inter-laminar currents are highly dependent on the properties of the cutting burr. At the cutting burr, the insulation layer of the electric steel is damaged. The cutting burr corrodes over time and the conductivity through the additional eddy current paths I_{ec} through the burr is reduced. Hence the corrosion of the cutting burr influences the additional Foucault eddy current losses.

When measuring the sample six months after cutting the cores, the loss increase at 1 kHz due to axial pressure is reduced from 44 % (six weeks after cutting) to 26.5 %.

To study the influence of additional inter-laminar eddy current paths, an additional insulation layer is added to every lamination. The thickness of this layer is 60 µm, which is the same as the largest measured height of the cutting burr. After disassembling the ring core and adding the insulation layer (c), the ring core was assembled and remeasured (Fig. 14). At 1 kHz, the loss increase due to axial pressure is reduced from 41.6 % to 20.3 %. Still the loss increase at high frequencies is significant. Hence, the ring core is disassembled again and the steel laminations are deburred. Since the insulation layer is damaged from the deburring process, an additional 60 µm insulation layer is applied. The deburred and insulated steel laminations are stacked and inserted in the winding body. The deburred ring core (d) is measured again (Fig. 15). Since the deburring changes the property of the cutting edge, the measurement results after deburring cannot be compared directly to the results before deburring. From 0 MPa to 10 MPa a 4.8 % increase of iron losses is measured at 1 kHz (Fig. 15).

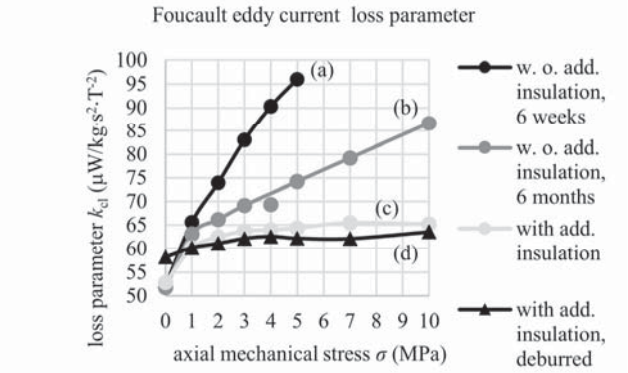

Fig. 17: Identified Foucault eddy current loss parameter k_{cl} (7) in dependency of axial mechanical pressure ($k_{ex} = 0.7\ \mathrm{mW \cdot kg^{-1} \cdot T^{-1.5} \cdot s^{-1.5}}$ = const.).

From the measurements at different frequency and flux density values, the iron loss parameter $k_{cl}(\sigma)$ is fitted according to (9). This is done for the measurements of the steel laminations before applying additional insulation (a,b), after applying the additional insulation layer (c), and after deburring (d). Fig. 16 shows the Foucault (macroscopic) eddy current loss parameters for the four different states of the laminations in dependency of the axial mechanical pressure σ. From Fig. 15 the influence of axial pressure on the Foucault eddy current losses is clarified. Analyzing the Foucault loss parameter for the measurement without additional insulation shows that the Foucault eddy current losses increase monotonic from $\sigma = 0$ MPa to $\sigma = 10$ MPa. The increase of k_{cl} from $\sigma = 0$ MPa to $\sigma = 10$ MPa is 67.3 %. The gradient of $\Delta k_{cl}/\Delta\sigma$ is the steepest from $\sigma = 0$ MPa to $\sigma = 1$ MPa with $\Delta k_{cl}/\Delta\sigma = 11.3\ \mathrm{\mu W \cdot kg^{-1} \cdot T^{-2} \cdot s^{-2} \cdot MPa^{-1}}$. From $\sigma = 1$ MPa to $\sigma = 10$ MPa the gradient $\Delta k_{cl}/\Delta\sigma$ is almost constant with a value of $\Delta k_{cl}/\Delta\sigma = 2.61\ \mathrm{\mu W \cdot kg^{-1} \cdot T^{-2} \cdot s^{-2} \cdot MPa^{-1}}$.

For the measurements, after applying the 60 µm insulation layer, the Foucault loss parameter increases less with the axial pressure σ. From $\sigma = 0$ MPa to $\sigma = 10$ MPa, k_{cl} increases by 23.5 %. The largest increase of k_{cl} is found between $\sigma = 0$ MPa and $\sigma = 2$ MPa. For $\sigma = 3$ MPa to $\sigma = 10$ MPa k_{cl} is almost constant with a difference of less than 2.7 %. The loss increase is drastically reduced by the additional insulation layer.

The identified Foucault loss parameter for the measurements after deburring and applying the second additional insulation layer of 60 µm is increased by 9.2 % from $\sigma = 0$ MPa to $\sigma = 10$ MPa.

V. Influence of Axial Pressure on Electrical Machine Characteristics

The measured magnetization curves are applied to 2D-FEM simulation of a 50 kW PMSM with V-shaped permanent magnets (VPMSM).

The rotor lamination stack is compressed by the axial forces, creating a denser rotor core. This effect is dependent on the thickness of the steel, the stamping process and the joining process of the rotor laminations. Interlocking is a widely used joining process for laminations. Since the soft magnetic measurement setup (Fig. 4) has a limited stiffness, the compression could not be measured using this setup and has to be considered by additional measurements. Hence, lamination stacks of a rotor made by interlocking of 0.35 mm laminations are compressed by means of axial pressure and the strain ε is measured (Fig. 1). At $\sigma = 4$ MPa, an increase of packing density of 2.6 % (i.e. $\varepsilon = 2.6$ %) is measured. This gives the possibility to insert more laminations into the rotor. In the soft magnetic measurement results from the setup in Fig. 4 the influence of strain ε is not incorporated. Hence the influence of strain ε on the magnetic flux density B is modelled according to:

$$\begin{aligned} B(\varepsilon, H) &= J(\varepsilon = 0, H) \cdot \frac{1}{1-\varepsilon} + H \cdot \mu_0 \\ &= \left(B(\varepsilon = 0, H) - H \cdot \mu_0 \right) \cdot \frac{1}{1-\varepsilon} + H \cdot \mu_0 . \end{aligned} \quad (10)$$

Fig. 18 shows the magnetization curves obtained by (10). At high values of $H > 1200$ A/m, higher values of magnetic flux density B are reached at $\sigma = 4$ MPa due to the axial strain of $\varepsilon = 2.6$ %. At $H < 1200$ A/m, the increase of the magnetic polarization J due to $\varepsilon = 2.6$ % is smaller than the reduction of

magnetizability from compressive pressure. As a result, the magnetic flux density B is smaller at values of $H < 1200$ A/m compared to a material without applied axial pressure (Fig. 18).

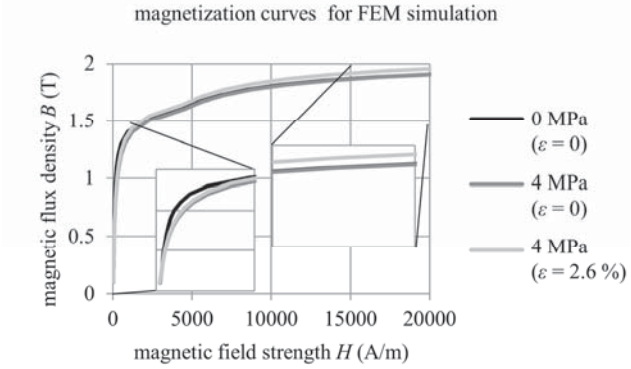

Fig. 18: Magnetization curves used for FEM simulation.

To find the impact of the change of the magnetization curves on machine behavior, the magnetization curves are applied to 2D-FEM simulations of a VPMSM. Simulations with variation of direct and quadrature stator current are conducted as described in [12]. From these simulations, the loss minimal operating points of direct and quadrature current are found for every combination of torque T and speed n. The simulated difference in stator current < 0.3 A is in every operating point of the machine. When compared to the maximum current of 300 A, the influence of the magnetization characteristics due to axial pressure has a small influence on the machine characteristics.

Since the rotor iron losses are dominated by the eddy current losses from slot harmonics, the rotor iron losses are highly dependent on the Foucault and excess eddy current losses. The iron loss model is applied to the local and temporal magnetic flux density distribution in the machine:

$$P_{\mathrm{Fe}} = m \cdot \left(k_{\mathrm{hy}} \cdot \sum_{\mathrm{n}} B_{\mathrm{n}}^{\alpha} f_{\mathrm{n}} + k_{\mathrm{ex}} \cdot \sum_{\mathrm{n}} B_{\mathrm{n}}^{1.5} f_{\mathrm{n}}^{1.5} + k_{\mathrm{cl}}(\sigma) \cdot \sum_{\mathrm{n}} B_{\mathrm{n}}^{2} f_{\mathrm{n}}^{2} \right) \quad (11)$$

The magnetic flux density in every element of the stator and rotor core is Fourier transformed. The Fourier transformation gives the magnitude B_{n} for every frequency f_{n} in every element of the 2D mesh. From the iron loss parameter with and without axial pressure, the difference in losses is studied.

For the Foucault eddy current losses, the identified Foucault loss parameter for the measurement without additional insulation (a) is used for value of $\sigma = 4$ MPa (Fig. 17). For the excess loss parameter a constant value of $k_{\mathrm{ex}} = 0.7\ \mathrm{mW \cdot kg^{-1} \cdot T^{-1.5} \cdot s^{-1.5}}$ is used as detailed in Section D. Subtracting the rotor iron losses at $\sigma = 0$ MPa from the rotor iron losses at $\sigma = 4$ MPa gives the increase of the rotor iron losses:

$$\Delta P_{\mathrm{Fe},2}(n,T,\sigma) = P_{\mathrm{Fe},2}(n,T,\sigma) - P_{\mathrm{Fe},2}(n,T,\sigma=0). \quad (12)$$

Fig. 19 shows the simulated increase of $\Delta P_{\mathrm{Fe},2}(\sigma = 4\ \mathrm{MPa})$ in dependency of n and T. As the rotor iron losses, the loss increase with n and T. The highest value of $\Delta P_{\mathrm{Fe},2}(\sigma = 4\ \mathrm{MPa}) = 220$ W is simulated at maximum speed $n_{\mathrm{max}} = 8{,}000$ rpm and the highest torque at this speed $T = 90$ Nm.

Fig. 20 shows the simulated increase of the power losses $\Delta P(\sigma = 4\ \mathrm{MPa})$ referred to power losses at $\sigma = 0$ MPa. The highest relative increase of power losses 4.5 % is found at $n_{\mathrm{max}} = 8{,}000$ rpm and $T = 90$ Nm. At a speed of 4,000 rpm and torque of 50 Nm an increase of almost 4 % is simulated.

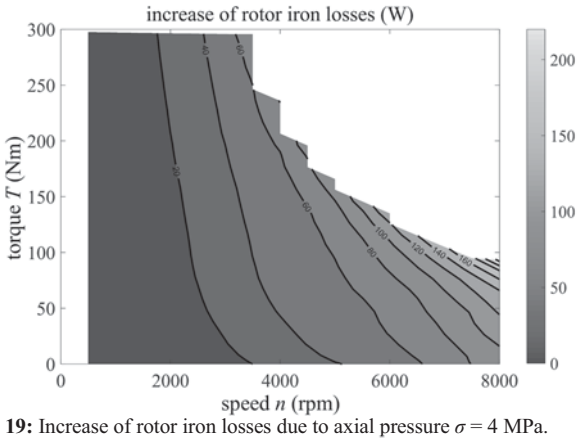

Fig. 19: Increase of rotor iron losses due to axial pressure $\sigma = 4$ MPa.

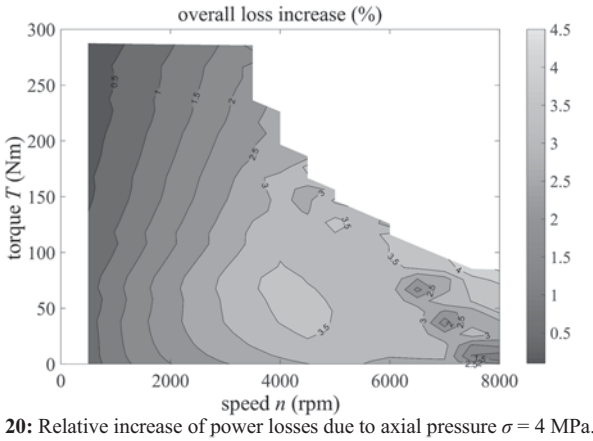

Fig. 20: Relative increase of power losses due to axial pressure $\sigma = 4$ MPa.

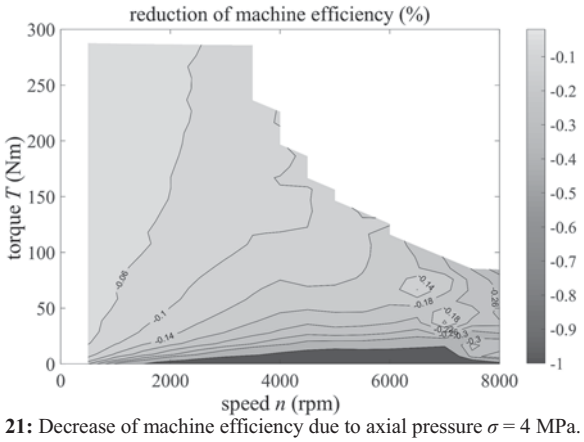

Fig. 21: Decrease of machine efficiency due to axial pressure $\sigma = 4$ MPa.

To find the influence of axial pressure σ on the efficiency η of the VPMSM, the difference of $\eta(n,T,\sigma = 4\ \mathrm{MPa})$ and $\eta(n,T,\sigma = 0)$ is calculated (Fig. 21). The relative increase of machine power losses (Fig. 20) and difference in efficiency (Fig. 21) are calculated by difference of the simulated value to the reference simulation. At 6,500 rpm to 7,500 rpm, three numerical artefacts from discretizing to torque and speed under the maximum voltage limitation are apparent. The influence of the increased iron losses on the machine efficiency is of least interest at operating points where the Ohmic losses dominate the power losses. At high torque and low speed, the influence of $\sigma = 4$ MPa on η is less than 0.1 %. The highest influence on η is found in the low load operation with small torque T. Since at low torque the efficiency of the machine is small, the influence of η is assessed having a small impact. At the highest speed

n_{max} = 8,000 rpm and T = 90 Nm, the machine efficiency is reduced by 0.5 %. Since the iron loss parameters are identified for the measurements (a) of the ring core with 60 µm cutting burr, 6 weeks after cutting by waterjet, the loss increase from axial pressure is a worst case estimation. Commonly produced machines can feature axial pressure $\sigma > 0$ to prevent the rotor stack from fanning apart and to create a more compact core. Hence, the comparison of the losses simulated with σ = 4 MPa to σ = 0 MPa is a worst case analysis. The ring core samples were prepared by waterjet cutting with a burr height of 60 µm. For laminations with lower burr height (e.g. created by stamping or laser cutting) the influence of axial pressure on eddy current losses will be smaller. Hence the increase of power losses and decrease of efficiency would be reduced.

VI. Conclusions

The influence of axial forces from a new rotor design that features axial torque propagation through axial compression discs are studied through soft magnetic measurements and 2D machine simulations.

No permanent influence of short time axial mechanical pressure on the magnetization or loss characteristics of electrical steel was measured.

Drastically increased (+53.8 %) iron losses were measured at high frequency (2 kHz) when applying axial pressure to the ring-core measurement setup. This drastic increase is not described in the literature studying axial pressure influences on the core losses of electrical machines [7 - 9]. The drastic loss increase is caused by additional Foucault eddy current losses from inter-laminar short circuit due to cutting burrs. When removing the cutting burrs and adding additional insulation between the laminations, the maximum loss increase was reduced to 7.4 %. The influence of axial pressure on the excess losses was identified to be small. When not removing the cutting burr or adding additional insulation between the electrical steel laminations, the loss increasing effect from axial pressure is not linear. Application of a relatively small axial pressure leads to the largest increase of the measured losses whereas increasing a high value of axial pressure increases the losses only minimal.

The identified iron loss parameters are applied to a 2D FE magnetic simulation of a 50 kW PMSM. In the rotor an axial pressure of 4 MPa was simulated. In the stator no axial pressure is applied. For the FE simulation, the iron loss parameters without any additional insulation layer were used. From the FE simulation, the influence of reduced magnetizability of the steel on the machine characteristics are found to be very small. However, the losses, due to increase of rotor iron losses from axial pressure, increase by a maximum of 4.5 % in this worst case scenario.

In the FE simulation, we imply a cutting burr of 60 µm. Measurements of machines without and with axial mechanical pressure can be conducted to measure the influence directly in the target application. The corrosion of the cutting burr and the consequential decreased electric conductivity between the lamination layers are possible future research topics.

In large electrical generators and motors, inter-laminar eddy currents through damages of the soft magnetic laminations are a cause for (total) machine failure [13, 14]. In electrical machines the cores are often compressed by means of axial pressure to stabilize the cores and prevent vibration of the laminations.

In [15] it is found that cutting non-oriented electric steel by water jet deteriorates the magnetic properties less than laser cutting. However this assumption is only valid when the laminations are not compressed by axial force and additional inter-laminar eddy current paths are created.

The measurement setup presented in this paper can be used to identify the maximum acceptable cutting burr height for machines with axial forces in stator or rotor.

References

[1] D. Singh, P. Rasilo, F. Martin, A. Belahcen and A. Arkkio, "Effect of Mechanical Stress on Excess Loss of Electrical Steel Sheets," in IEEE Transactions on Magnetics, vol. 51, no. 11, pp. 1-4, Nov. 2015.

[2] Y. Kai, Y. Tsuchida, T. Todaka and M. Enokizono, "Influence of Stress on Vector Magnetic Property Under Alternating Magnetic Flux Conditions," in IEEE Transactions on Magnetics, vol. 47, no. 10, pp. 4344-4347, Oct. 2011.

[3] V. Permiakov, A. Pulnikov, L. Dupre and J. Melkebeek, "Rotational magnetization in nonoriented Fe-Si steel under uniaxial compressive and tensile stresses," in IEEE Transactions on Magnetics, vol. 40, no. 4, pp. 2760-2762, July 2004.

[4] A. Poulnikov, V. Permiakov, M. De Wulf, L. Dupre, D. Makaveev and J. Melkebeek, "Investigation of residual effects of tensile stress on magnetic properties of nonoriented electrical steel," in IEEE Transactions on Magnetics, vol. 38, no. 5, pp. 3204-3206, Sep. 2002.

[5] K. Fujisaki and S. Satoh, "Numerical calculations of electromagnetic fields in silicon steel under mechanical stress," in IEEE Transactions on Magnetics, vol. 40, no. 4, pp. 1820-1825, Jul. 2004.

[6] K. Fujisaki et al., "Motor Core Iron Loss Analysis Evaluating Shrink Fitting and Stamping by Finite-Element Method," in IEEE Transactions on Magnetics, vol. 43, no. 5, pp. 1950-1954, May 2007.

[7] L. Vandenbossche, S. Jacobs, D. Van Hoecke and E. Attrazic, "Impact of mechanical stresses on the magnetic performance of non-oriented electrical steels and its relation to electric machine efficiency," *Transportation Electrification Conference and Expo (ITEC),* Dearborn, MI, 2015.

[8] N. Mimura, N. Takahashi, M. Nakano, D. Miyagi, M. Kawabe, T. Nomiyama, A. Siozaki, "Effect of Specimen Shape on Magnetic Properties under Compressive Stress in Thickness Direction of Non-oriented Electrical Steel Sheet," The papers of Technical Meeting on Magnetics, IEE Japan, MAG-11-28, 2011.

[9] K.-I. Yamamoto and S. Yanase, "Effects of normal compressive stress on magnetic losses of non-oriented electrical steels," The papers of Technical Meeting on Magnetics, IEE Japan, MAG-09-225, 2009.

[10] A. Eldieb and F. Anayi, "Evaluation of Loss Generated by Edge Burrs in Electrical Steels," in IEEE Transactions on Magnetics, vol. 52, no. 5, pp. 1-4, May 2016.

[11] R. Mazurek, P. Marketos, A. Moses and J. N. Vincent, "Effect of Artificial Burrs on the Total Power Loss of a Three-Phase Transformer Core," in IEEE Transactions on Magnetics, vol. 46, no. 2, pp. 638-641, Feb. 2010.

[12] A. Ruf, A. Thul, S. Steentjes, and K. Hameyer, "Loss minimizing control strategy for electrical machines considering iron loss distribution," 2015 IEEE International Electric Machines & Drives Conference (IEMDC), Coeur d'Alene, ID, pp. 974-980, May 2015.

[13] "IEEE Guide for Insulation Maintenance of Large Alternating-Current Rotating Machinery (10,000 kVA and Larger)," in ANSI/IEEE Std 56-1977 , Mar. 1977.

[14] G. B. Kliman, Sang Bin Lee, M. R. Shah, R. M. Lusted and N. K. Nair, "A new method for synchronous generator core quality evaluation," in *IEEE Transactions on Energy Conversion*, vol. 19, no. 3, pp. 576-582, Sept. 2004.

[15] V. M. Paltanea, G. Paltanea and H. Gavrila, "Some important effects of the water jet and laser cutting methods on the magnetic properties of the non-oriented silicon iron sheets," *9th International Symposium on Advanced Topics in Electrical Engineering (ATEE)*, Bucharest, pp. 452-455, May 2015.